ELSEVIER

On the accuracy of the self-consistent approximation for polycrystals: comparison with full-field numerical simulations

R.A. Lebensohn [a,*], Y. Liu [b], P. Ponte Castañeda [b]

[a] *Materials Science and Technology Division, Los Alamos National Laboratory, Los Alamos, NM 87845, USA*
[b] *Department of Mechanical Engineering and Applied Mechanics, University of Pennsylvania, Philadelphia, PA 19104-6315, USA*

Abstract

This paper presents comparisons between full-field numerical results and self-consistent (SC) estimates for the effective behavior and statistical fluctuations of the stress and strain-rate fields in viscoplastic polycrystals. The full-field simulations make use of a recently introduced technique, based on the fast Fourier transform (FFT) algorithm. Applications are given for linear and power-law polycrystals with randomly distributed FCC and HCP grains. For linear systems, the FFT results demonstrate the accuracy of the standard SC approximation, even for relatively large values of the grain anisotropy parameter when the field fluctuations become significant. On the other hand, of the various extensions of the self-consistent method that have been proposed for nonlinear systems, the recent 'second-order' method appears to give the best overall predictions for both the effective behavior and the statistical fluctuations of the stress and strain-rate fields in power-law polycrystals.
Published by Elsevier Ltd on behalf of Acta Materialia Inc.

Keywords: Polycrystals; Power-law slip; Self-consistent theory; Effective behavior; Field fluctuations

1. Introduction

The self-consistent approximation, originally proposed by Hershey [1] and Kröner [2] for linear elastic materials, is by far the most commonly used method for estimating the macroscopic behavior of polycrystalline aggregates—both linear and nonlinear. For linear systems, where several different interpretations and derivations have been given (e.g. [3,4]), the various self-consistent approximations all lead to essentially the same result, at least for untextured polycrystals with 'equiaxed' grains. On the other hand, for nonlinear systems, the many different extensions of the self-consistent approximation that have been proposed in the literature all give widely diverging predictions. For example, the 'incremental' method of Hill [5] and Hutchinson [6] becomes close to the Taylor upper bound estimate for low rate-sensitivity materials, while the 'tangent' procedure of Molinari et al. [7] and Lebensohn and Tomé [8] leads to estimates that are close to the Reuss lower bound estimate in this case. For polycrystals with large grain anisotropy, these estimates can therefore lead to large differences in the predictions for the macroscopic behavior of such materials.

Given that many materials, natural and man-made, are polycrystals, it is of great interest to assess the accuracy of the various self-consistent approximations. In this work, we propose to do precisely this, by making comparisons of these self-consistent (SC) approximations with the results of numerical simulations over ensembles of polycrystals with random microstructures. To accomplish this, we make use of a technique based

* Corresponding author. Tel.: +1 505 665 3035; fax: +1 505 667 8021.
E-mail address: lebenso@lanl.gov (R.A. Lebensohn).

on the use of fast Fourier transforms (FFT) proposed originally by Moulinec and Suquet [9,10], developed further by Michel et al. [11], and first applied to polycrystals by Lebensohn [12], Lebensohn et al. [13] and Bhattacharya and Suquet [14]. In some sense, this paper is a continuation of our earlier work [13], where we were able to perform similar comparisons for a certain class of two-dimensional (2-D) model polycrystals. Here, we first consider the case of random three-dimensional (3-D) polycrystals with linear behavior, where all the self-consistent formulations agree, and attempt to verify the accuracy of the self-consistent approximation in this case. This check is essential also because all the nonlinear extensions of the self-consistent model make use of the results of the linear formulation, in some form or another.

Having verified the accuracy of the approximation for several representative linear systems, including polycrystals with FCC and HCP grains, we proceed to compare the two above-mentioned nonlinear extensions (i.e. 'incremental' and 'tangent'), as well as some more recently proposed methods, based on rigorous homogenization theories, with corresponding FFT simulations, for ensembles of FCC and ice (HCP) polycrystals with power-law viscous behavior and isotropic textures. More specifically, these recent extensions of the self-consistent approximation are based on the use of variational 'linear comparison' methods, which express the effective potential of the nonlinear viscoplastic polycrystal in terms of that of a linearly viscous polycrystal with properties that are determined from suitably designed variational principles. Two types of estimates are available depending on the method used. The first is based on the 'variational' method of Ponte Castañeda [15,16], and the second on the 'second-order' method of the same author [17,18]. These methods have the advantage that they incorporate information not only on the average fields in the grains, but in addition, also on the second moments, or field fluctuations [19]. It should be noted that there is an earlier version of the second-order method [20] (called in what follows 'second-order NF'), which neglects the field fluctuations. Finally, the recently proposed 'affine' method of Masson et al. [21], which will be used in some of the comparisons presented in this work, can be viewed as a simplified version of the 'second-order NF' method, where the overall behavior is obtained directly from the stress-strain relation for the relevant linear comparison composite, which happens to be identical for both methods.

In addition to comparing the effective (macroscopic) behavior, we also compare grain averages, as well as higher-order statistical information in the form of the stress and strain fluctuations within the polycrystal. These fluctuations serve to characterize the heterogeneity of the fields within the polycrystal, which could be useful to generate improved estimations of the micro-

structure evolution that is generated by the internal fields in these materials when they are subjected to external loading. They could also be useful in predicting damage.

2. Polycrystals and effective behavior

By 'polycrystals' in this work we mean random, statistically homogeneous aggregates of perfectly bonded single-crystal grains with varying orientations. For simplicity, the grain orientations will be assumed to take on a set of discrete values, defined by rotation tensors $\mathbf{Q}^{(r)}$ $(r = 1, \ldots, N)$. Then, the grains with a given orientation $\mathbf{Q}^{(r)}$ occupy 'phases' $\Omega^{(r)}$ $(r = 1, \ldots, N)$, such that $\Omega = \cup_{r=1}^{N} \Omega^{(r)}$. Their functions $\chi^{(r)}$, serving to describe the location of the various orientations, are defined to be equal to 1 if the position vector $\mathbf{x}$ is in $\Omega^{(r)}$ and zero otherwise. Volume averages over Ω, and over phase $\Omega^{(r)}$ are denoted by $\langle \cdot \rangle$ and $\langle \cdot \rangle^{(r)}$, respectively. The phase probabilities $c^{(r)} = \langle \chi^{(r)} \rangle$ serve to characterize the crystallographic texture of the aggregate.

The local constitutive response of the polycrystal is defined by the relations

$$\boldsymbol{\varepsilon} = \frac{\partial u}{\partial \boldsymbol{\sigma}}, \quad u(\mathbf{x}, \boldsymbol{\sigma}) = \sum_{r=1}^{N} \chi^{(r)}(\mathbf{x}) u^{(r)}(\boldsymbol{\sigma}),$$

$$u^{(r)}(\boldsymbol{\sigma}) = \sum_{k=1}^{K} \phi_{(k)}^{(r)} \left(\tau_{(k)}^{(r)} \right), \tag{1}$$

where $\boldsymbol{\sigma}$ is the Cauchy stress, $\boldsymbol{\varepsilon}$ is the Eulerian strain-rate, and u and $u^{(r)}$ are the stress potentials for the polycrystal and single crystals with orientation $\mathbf{Q}^{(r)}$, respectively. The slip potentials $\phi_{(k)}^{(r)}$ $(k = 1, \ldots, K)$ characterize the response of the K slip systems in the crystals with orientation $\mathbf{Q}^{(r)}$ and depend on the resolved shear (or Schmid) stresses

$$\tau_{(k)}^{(r)} = \boldsymbol{\sigma} \cdot \boldsymbol{\mu}_{(k)}^{(r)}, \quad \boldsymbol{\mu}_{(k)}^{(r)} = \frac{1}{2} \left(\mathbf{n}_{(k)}^{(r)} \otimes \mathbf{m}_{(k)}^{(r)} + \mathbf{m}_{(k)}^{(r)} \otimes \mathbf{n}_{(k)}^{(r)} \right). \tag{2}$$

Here, the $\boldsymbol{\mu}_{(k)}^{(r)}$ are second-order tensors with $\mathbf{n}_{(k)}^{(r)}$ and $\mathbf{m}_{(k)}^{(r)}$ denoting the unit vectors normal to the slip plane and along the slip direction of the kth system, respectively, for crystals with orientation $\mathbf{Q}^{(r)}$. For this class of viscoplastic polycrystals, it is known [6] that the effective response, characterizing the relation between the average strain-rate $\bar{\boldsymbol{\varepsilon}} = \langle \boldsymbol{\varepsilon} \rangle$ and the average stress $\bar{\boldsymbol{\sigma}}$, is determined by

$$\bar{\boldsymbol{\varepsilon}} = \frac{\partial \widetilde{U}}{\partial \bar{\boldsymbol{\sigma}}}, \quad \widetilde{U}(\bar{\boldsymbol{\sigma}}) = \min_{\boldsymbol{\sigma} \in \mathscr{S}(\bar{\boldsymbol{\sigma}})} \langle u(\mathbf{x}, \boldsymbol{\sigma}) \rangle = \min_{\boldsymbol{\sigma} \in \mathscr{S}(\bar{\boldsymbol{\sigma}})} \sum_{r=1}^{N} c^{(r)} \langle u^{(r)}(\boldsymbol{\sigma}) \rangle^{(r)}, \tag{3}$$

where $\widetilde{U}$ is the effective stress potential for the polycrystal, and $\mathscr{S}(\bar{\boldsymbol{\sigma}}) = \{ \boldsymbol{\sigma}, \text{ such that div } \boldsymbol{\sigma} = \mathbf{0} \text{ and } \langle \boldsymbol{\sigma} \rangle = $

$\bar{\boldsymbol{\sigma}}$ in Ω} denotes the set of statically admissible stresses consistent with an average stress $\bar{\boldsymbol{\sigma}}$.

For simplicity, the slip potentials of the grains with various orientations will be taken to be identical, i.e. $\phi_{(k)}^{(r)} = \phi_{(k)}$, and use will be made here of the standard power-law form for these slip potentials

$$\phi_{(k)}(\tau) = \frac{\gamma_0 (\tau_0)_{(k)}}{n+1} \left| \frac{\tau}{(\tau_0)_{(k)}} \right|^{n+1}, \tag{4}$$

where $m = 1/n$ ($0 \leqslant m \leqslant 1$) is the strain-rate sensitivity, $(\tau_0)_{(k)} > 0$ is the reference flow stress of the kth slip system, and γ_0 is a reference shear-rate. The fact that the viscous exponent n has been assumed to be the same for all the slip systems and all the grains in the polycrystal leads to the effective potential of the polycrystal $\widetilde{U}$ being a homogeneous function of degree $n + 1$ on the average stress $\bar{\boldsymbol{\sigma}}$. Additionally, since the polycrystal is incompressible, $\widetilde{U}$ will depend on $\bar{\boldsymbol{\sigma}}$ only through its deviator $\bar{\mathbf{s}}$ (i.e. it is independent of $\bar{\sigma}_m = \frac{1}{3} \mathrm{tr}\, \bar{\boldsymbol{\sigma}}$). Introducing the von Mises equivalent stress $\bar{\sigma}_e = \sqrt{\frac{3}{2} \bar{\mathbf{s}} \cdot \bar{\mathbf{s}}}$, it follows that:

$$\widetilde{U}(\bar{\boldsymbol{\sigma}}) = \frac{\tilde{\sigma}_0}{(n+1)} \left(\frac{\bar{\sigma}_e}{\tilde{\sigma}_0} \right)^{n+1}, \tag{5}$$

where the effective flow stress of the polycrystal, denoted $\tilde{\sigma}_0$, depends, in general, on both the loading and the microstructure of the polycrystal.

For later use, some additional notation is introduced next. The per-phase (over grains with orientation r) averages of the stress and strain-rate are defined via $\bar{\boldsymbol{\sigma}}^{(r)} = \langle \boldsymbol{\sigma} \rangle^{(r)}$ and $\bar{\boldsymbol{\varepsilon}}^{(r)} = \langle \boldsymbol{\varepsilon} \rangle^{(r)}$, and are such that $\bar{\boldsymbol{\sigma}} = \sum_{r=1}^{N} c^{(r)} \bar{\boldsymbol{\sigma}}^{(r)}$ and $\bar{\boldsymbol{\varepsilon}} = \sum_{r=1}^{N} c^{(r)} \bar{\boldsymbol{\varepsilon}}^{(r)}$. The von Mises equivalent measures associated with $\bar{\boldsymbol{\sigma}}^{(r)}$ and $\bar{\boldsymbol{\varepsilon}}^{(r)}$ are defined by: $\bar{\sigma}_e^{(r)} = \sqrt{\frac{3}{2} \bar{\mathbf{s}}^{(r)} \cdot \bar{\mathbf{s}}^{(r)}}$, where $\bar{\mathbf{s}}^{(r)}$ is the average stress deviator in phase r, and $\bar{\varepsilon}_e^{(r)} = \sqrt{\frac{2}{3} \bar{\boldsymbol{\varepsilon}}^{(r)} \cdot \bar{\boldsymbol{\varepsilon}}^{(r)}}$, respectively. In addition, the second moments of the stress and strain-rate over phase r are given by $\langle \boldsymbol{\sigma} \otimes \boldsymbol{\sigma} \rangle^{(r)}$ and $\langle \boldsymbol{\varepsilon} \otimes \boldsymbol{\varepsilon} \rangle^{(r)}$, in terms of which expressions may be obtained for the corresponding phase fluctuation covariance tensors

$$\mathbf{C}_{\boldsymbol{\sigma}}^{(r)} := \left\langle \left(\boldsymbol{\sigma} - \bar{\boldsymbol{\sigma}}^{(r)} \right) \otimes \left(\boldsymbol{\sigma} - \bar{\boldsymbol{\sigma}}^{(r)} \right) \right\rangle^{(r)}$$
$$= \langle \boldsymbol{\sigma} \otimes \boldsymbol{\sigma} \rangle^{(r)} - \bar{\boldsymbol{\sigma}}^{(r)} \otimes \bar{\boldsymbol{\sigma}}^{(r)}, \tag{6}$$

and similarly for $\mathbf{C}_{\boldsymbol{\varepsilon}}^{(r)}$. In particular, use will be made here of the standard deviation (SD) of the von Mises stress and the equivalent plastic strain-rate over phase r [13]

$$\mathrm{SD}^{(r)}(\sigma_e) = \sqrt{\left\langle \sigma_e^2 - \left(\bar{\sigma}_e^{(r)} \right)^2 \right\rangle^{(r)}},$$

$$\mathrm{SD}^{(r)}(\varepsilon_e) = \sqrt{\left\langle \varepsilon_e^2 - \left(\bar{\varepsilon}_e^{(r)} \right)^2 \right\rangle^{(r)}}. \tag{7}$$

Completely analogous expressions may be given for the overall (polycrystal-wide) fluctuation covariance tensors $\mathbf{C}_{\boldsymbol{\sigma}}$ and $\mathbf{C}_{\boldsymbol{\varepsilon}}$, as well as for the overall standard deviations

SD(σ_e) and SD(ε_e) [13]. For instance, SD$(\sigma_e) = \sqrt{\langle \sigma_e^2 - \bar{\sigma}_e^2 \rangle}$, but note that $\mathrm{SD}(\sigma_e) \neq \sum_{r=1}^{N} c^{(r)} \mathrm{SD}^{(r)}(\sigma_e)$.

3. Self-consistent estimates for effective behavior

3.1. Linear polycrystals

This section is concerned with polycrystals with linear constitutive behavior. The discussion applies equally well to linear elastic and linearly viscous systems, provided that the symbols appearing in the relevant equations are given appropriate physical interpretations. For reasons that will become evident further below, the behavior of the linear heterogeneous materials of interest in this section will be enlarged slightly to include 'thermoelastic' behavior characterized by constitutive relations of the type

$$\boldsymbol{\varepsilon} = \mathbf{M}^{(r)} \boldsymbol{\sigma} + \mathbf{e}^{(r)}, \quad u^{(r)}(\boldsymbol{\sigma}) = \frac{1}{2} \boldsymbol{\sigma} \cdot \mathbf{M}^{(r)} \boldsymbol{\sigma} + \mathbf{e}^{(r)} \cdot \boldsymbol{\sigma}, \tag{8}$$

where $\mathbf{M}^{(r)}$ and $\mathbf{e}^{(r)}$ define the viscous compliance tensor and 'thermal' strain-rate tensor of phase r. Because of the linearity of the problem, it is known [22] that the average of the stress over phase r in this linear comparison 'thermoelastic' composite may be written in the form

$$\bar{\boldsymbol{\sigma}}^{(r)} = \mathbf{B}^{(r)} \bar{\boldsymbol{\sigma}} + \mathbf{b}^{(r)}, \tag{9}$$

where $\mathbf{B}^{(r)}$ and $\mathbf{b}^{(r)}$ are concentration tensors depending on the homogenization procedure utilized. Using these concentration tensors, the effective potential $\widetilde{U}_T$ of this linear composite may be written in the form [18]

$$\widetilde{U}_T(\bar{\boldsymbol{\sigma}}) = \frac{1}{2} \bar{\boldsymbol{\sigma}} \cdot \widetilde{\mathbf{M}} \bar{\boldsymbol{\sigma}} + \tilde{\mathbf{e}} \cdot \bar{\boldsymbol{\sigma}} + \frac{1}{2} \tilde{g}, \tag{10}$$

where $\widetilde{\mathbf{M}} = \sum_{r=1}^{N} c^{(r)} \mathbf{M}^{(r)} \mathbf{B}^{(r)}$, $\tilde{\mathbf{e}} = \sum_{r=1}^{N} c^{(r)} \mathbf{B}^{(r)T} \mathbf{e}^{(r)}$, $\tilde{g} = \sum_{r=1}^{N} c^{(r)} \mathbf{b}^{(r)} \cdot \mathbf{e}^{(r)}$ are the effective compliance, effective 'thermal' strain-rate and effective energy under zero applied stress, respectively. Note that the associated effective stress–strain-rate relation is given by

$$\bar{\boldsymbol{\varepsilon}} = \widetilde{\mathbf{M}} \bar{\boldsymbol{\sigma}} + \tilde{\mathbf{e}}. \tag{11}$$

Self-consistent estimates for thermoelastic systems are available from the works of Laws [22] and Willis [23]. Explicit expressions of the concentration tensors $\mathbf{B}^{(r)}$ and $\mathbf{b}^{(r)}$ tensors for the case 'equiaxed' grains can be found in reference [18]. Given those concentration tensors, corresponding estimates may be generated for the phase averages $\bar{\boldsymbol{\sigma}}^{(r)}$ and the effective potential $\widetilde{U}_T$ of the linear comparison polycrystal. In addition, estimates for the second moments of the stress over phase r may be obtained by means of the formula [24–26]

$$\langle \boldsymbol{\sigma} \otimes \boldsymbol{\sigma} \rangle^{(r)} = \frac{2}{c^{(r)}} \frac{\partial \widetilde{U}_{\mathrm{T}}}{\partial \mathbf{M}^{(r)}}, \tag{12}$$

where the variables $\mathbf{e}^{(r)}$ are held fixed in the differentiation. Corresponding expressions for the phase fluctuation covariance tensors and standard deviations then follow using expressions (6) and (7).

For the special case of polycrystals with isotropic crystallographic and morphological textures, leading to overall isotropic properties, it is possible to simplify the above expressions, depending on the symmetry of the single crystals. The results for the effective behavior are standard [23] and will not be repeated here.

3.2. Nonlinear polycrystals

In this subsection, the 'second-order' homogenization method for viscoplastic polycrystals is briefly recalled [18]. The key idea of the method is to introduce a 'linear thermoelastic comparison polycrystal' with local behavior defined by relations (8), where the viscous compliance and 'thermal' strain-rate tensors are written

$$\mathbf{M}^{(r)} = \sum_{k=1}^{K} \alpha_{(k)}^{(r)} \boldsymbol{\mu}_{(k)}^{(r)} \otimes \boldsymbol{\mu}_{(k)}^{(r)} \quad \text{and}$$

$$\mathbf{e}^{(r)} = \sum_{k=1}^{K} e_{(k)}^{(r)} \boldsymbol{\mu}_{(k)}^{(r)}, \tag{13}$$

in terms of corresponding slip-level quantities $\alpha_{(k)}^{(r)}$ and $e_{(k)}^{(r)}$, respectively. Approximating the local potential of the nonlinear polycrystal u in terms of the local potential of this linear comparison polycrystal, Liu and Ponte Castañeda [18] generated the following approximation for the effective potential of the nonlinear polycrystal:

$$\widetilde{U}(\bar{\boldsymbol{\sigma}}) = \sum_{r=1}^{N} \sum_{k=1}^{K} c^{(r)} \left\{ \phi_{(k)}^{(r)}\left(\hat{\tau}_{(k)}^{(r)}\right) + \phi_{(k)}^{(r)\prime}\left(\bar{\tau}_{(k)}^{(r)}\right)\left(\bar{\tau}_{(k)}^{(r)} - \hat{\tau}_{(k)}^{(r)}\right) \right\}, \tag{14}$$

where the variables $\bar{\tau}_{(k)}^{(r)}$ and $\hat{\tau}_{(k)}^{(r)}$ depend on the averages and fluctuations of the resolved shear stress $\tau_{(k)}^{(r)}$ on the slip system k for grain orientation r in the linear comparison polycrystal, defined by relations (8) and (13), in such a way that

$$\bar{\tau}_{(k)}^{(r)} := \left\langle \tau_{(k)}^{(r)} \right\rangle^{(r)} = \bar{\boldsymbol{\sigma}}^{(r)} \cdot \boldsymbol{\mu}_{(k)}^{(r)} \tag{15}$$

and

$$\left(\hat{\tau}_{(k)}^{(r)} - \bar{\tau}_{(k)}^{(r)}\right)^2 := \left\langle \left(\tau_{(k)}^{(r)} - \bar{\tau}_{(k)}^{(r)}\right)^2 \right\rangle^{(r)} = \boldsymbol{\mu}_{(k)}^{(r)} \mathbf{C}_{\boldsymbol{\sigma}}^{(r)} \cdot \boldsymbol{\mu}_{(k)}^{(r)}, \tag{16}$$

where the quantities $\hat{\tau}_{(k)}^{(r)} - \bar{\tau}_{(k)}^{(r)}$ are taken to have the same sign as the $\bar{\tau}_{(k)}^{(r)}$.

In turn, the variables $e_{(k)}^{(r)}$ and $\alpha_{(k)}^{(r)}$ in relations (13) for $\mathbf{e}^{(r)}$ and $\mathbf{M}^{(r)}$, defining the properties of the linear comparison polycrystal, are required to satisfy the closure relations [18]

$$e_{(k)}^{(r)} = \phi_{(k)}^{(r)\prime}\left(\bar{\tau}_{(k)}^{(r)}\right) - \alpha_{(k)}^{(r)}\bar{\tau}_{(k)}^{(r)} \tag{17}$$

and

$$\phi_{(k)}^{(r)\prime}\left(\hat{\tau}_{(k)}^{(r)}\right) - \phi_{(k)}^{(r)\prime}\left(\bar{\tau}_{(k)}^{(r)}\right) = \alpha_{(k)}^{(r)}\left(\hat{\tau}_{(k)}^{(r)} - \bar{\tau}_{(k)}^{(r)}\right). \tag{18}$$

4. Numerical simulations

4.1. The FFT approach

Moulinec and Suquet [9,10] developed an iterative method based on the FFT algorithm to compute the effective properties and the local fields of elastic and elastoplastic periodic composites. Lebensohn [12] used Moulinec-Suquet's FFT formulation to predict overall and local textures in viscoplastic polycrystals. However, as pointed out by Michel et al. [27] and Lebensohn [12], the original FFT iterative method is not well suited for materials with low rate-sensitivity and strongly anisotropic properties. To overcome this limitation, Michel et al. [11] proposed an improved FFT formulation for isotropic composites with high contrast of properties between phases, based on an augmented Lagrangian method. In an earlier work [13], we adapted this improved FFT formulation to deal with model 2-D polycrystals. In what follows, we give a brief explanation of the above augmented Lagrangian method. For a more detailed description of this formulation, the reader is referred to the works of Michel et al. [11,28] for composites, and to Lebensohn et al. [13] for polycrystals.

The FFT method is based on the solution of a unit cell problem with periodic boundary conditions. The unit cell under consideration should be discretized into $N_1 \times N_2 \times N_3$ Fourier points. This discretization determines a regular grid in the Cartesian space $\{\mathbf{x}_{\mathrm{d}}\}$ and a corresponding grid in the Fourier space $\{\boldsymbol{\xi}_{\mathrm{d}}\}$. The method also requires the selection of a linear reference medium of stiffness $\mathbf{L}^0$. Then, the Fourier transform of the Green operator $\hat{\boldsymbol{\Gamma}}^0(\boldsymbol{\xi})$ associated with this reference medium can be readily obtained for each point of Fourier grid [10,12]. Next, the FFT-based algorithm consists in finding a strain-rate field, associated with a kinematically admissible velocity field, that minimizes the average of the local strain energies, under the constraint imposed by the strain compatibility condition. If a macroscopic strain-rate $\bar{\boldsymbol{\varepsilon}}$ is imposed on the unit cell, the algorithm can be initialized under a uniform strain-rate assumption $\breve{\boldsymbol{\varepsilon}}^0(\mathbf{x}) = \mathbf{0} \; \forall \mathbf{x} \in \{\mathbf{x}_d\}$, where $\breve{\boldsymbol{\varepsilon}}^0(\mathbf{x})$ is the initial guess for the local strain-rate deviation field, i.e. $\breve{\boldsymbol{\varepsilon}}(\mathbf{x}) = \boldsymbol{\varepsilon}(\mathbf{x}) - \bar{\boldsymbol{\varepsilon}}$, and the corresponding initial guess of the stress field

$\boldsymbol{\sigma}^0(\mathbf{x})$ can be obtained from the local constitutive relation. Furthermore, it can be assumed that $\boldsymbol{\lambda}^0(\mathbf{x}) = \boldsymbol{\sigma}^0(\mathbf{x})$, where $\boldsymbol{\lambda}^0(\mathbf{x})$ is the initial guess for a field of Lagrange multipliers associated with the compatibility constraint. These initial field values can be used to start the iterative procedure that follows. If $\breve{\boldsymbol{\varepsilon}}^i(\mathbf{x})$ and $\boldsymbol{\lambda}^i(\mathbf{x})$ are known $\forall \mathbf{x} \in \{\mathbf{x}_d\}$, the $(i + 1)$th iteration starts with the calculation of the polarization field: $\boldsymbol{\delta}^{i+1}(\mathbf{x}) = \boldsymbol{\lambda}^i(\mathbf{x}) - \mathbf{L}^0 \breve{\boldsymbol{\varepsilon}}^i(\mathbf{x})$. Next, $\hat{\boldsymbol{\delta}}^{i+1}(\boldsymbol{\xi}) = fft\{\boldsymbol{\delta}^{i+1}(\mathbf{x})\}$ can be computed. The new guess for the kinematically admissible strain-rate deviation field can be then obtained as: $\hat{\breve{\epsilon}}^{i+1}(\boldsymbol{\xi}) = -\hat{\boldsymbol{\Gamma}}^0(\boldsymbol{\xi})\hat{\boldsymbol{\delta}}^i(\boldsymbol{\xi})$, $\forall \boldsymbol{\xi} \neq \mathbf{0}$, and $\hat{\breve{\epsilon}}^{i+1}(\mathbf{0}) = \mathbf{0}$. The corresponding field in real space $\breve{\epsilon}^{i+1}(\mathbf{x})$ is thus obtained by application of the inverse FFT, and the new guess for the deviatoric stress field is calculated from [11]

$$\boldsymbol{\sigma}^{i+1}(\mathbf{x}) + \mathbf{L}^0\boldsymbol{\varepsilon}^{i+1}(\mathbf{x}) = \boldsymbol{\lambda}^i(\mathbf{x}) + \mathbf{L}^0(\bar{\boldsymbol{\varepsilon}} + \breve{\epsilon}^{i+1}(\mathbf{x})), \qquad (19)$$

where $\boldsymbol{\varepsilon}^{i+1}(\mathbf{x})$ and $\boldsymbol{\sigma}^{i+1}(\mathbf{x})$ are related through the local constitutive equation. The latter is a system of nonlinear equations whose solution gives $\boldsymbol{\sigma}^{i+1}(\mathbf{x}) \ \forall \mathbf{x} \in \{\mathbf{x}_d\}$. To complete the iteration, the new guess of the Lagrange multiplier field is obtained from [11]

$$\boldsymbol{\lambda}^{i+1}(\mathbf{x}) = \boldsymbol{\lambda}^i(\mathbf{x}) + \mathbf{L}^0(\epsilon^{i+1}(\mathbf{x}) - \boldsymbol{\varepsilon}^{i+1}(\mathbf{x})). \qquad (20)$$

The convergence criterion after the jth iteration is thus given by

$$\text{err}(\boldsymbol{\sigma}) = \frac{\left\langle \|\boldsymbol{\sigma}^j(\mathbf{x}) - \boldsymbol{\lambda}^j(\mathbf{x})\|_2 \right\rangle}{\bar{\sigma}_e} < \delta,$$

$$\text{err}(\boldsymbol{\varepsilon}) = \frac{\left\langle \|\boldsymbol{\varepsilon}^j(\mathbf{x}) - \epsilon^j(\mathbf{x})\|_2 \right\rangle}{\bar{\varepsilon}_e} < \delta, \qquad (21)$$

where $\|\cdot\|_2$ denotes the quadratic norm, $\bar{\varepsilon}_e$ and $\bar{\sigma}_e$ are the macroscopic equivalent strain-rate and stress, and δ is a small positive threshold quantity. Expressions (19)–(21) guarantee the convergence of: (a) $\boldsymbol{\varepsilon}(\mathbf{x})$ (i.e. the strain-rate field related with the stress through the constitutive equation) towards $\epsilon(\mathbf{x})$ (i.e. the kinematically admissible strain-rate field) to fulfill compatibility, and (b) the Lagrange multiplier field $\boldsymbol{\lambda}(\mathbf{x})$ towards the stress field $\boldsymbol{\sigma}(\mathbf{x})$ to fulfill equilibrium.

4.2. Ensemble averages over FFT solutions

Just as in our previous work on 2-D polycrystals [13], the above FFT formulation has been used to obtain effective properties of isotropic polycrystals with random microstructure by means of ensemble averages, i.e. averages over the outcomes of 'numerical experiments' performed on many specimens which are generated alike, i.e. by random assignment of orientations to a given array of grains that constitutes a representative volume element, but differ at micro level, due to the inherent stochastic character of such generation procedure. Therefore, let us consider a periodic 3-D poly-

crystal, generated by periodic repetition of a cubic unit cell consisting of $8 \times 8 \times 8 = 512$ cubic grains of randomly chosen orientations. If this unit cell is in turn discretized using a $64 \times 64 \times 64$ Fourier grid, this results in $8 \times 8 \times 8 = 512$ Fourier points per grain. Such unit cell is representative of a periodic polycrystal generated by repetition of the unit cell in each direction of the space. The response of this periodic polycrystal is equivalent to that of one specimen in an ensemble. Therefore, the averages over a sufficiently large number of periodic unit cell configurations should give the effective properties of a polycrystal with random microstructure. It should be noted that the microstructures of these polycrystals, generated for ensemble averaging, are random only in a *restricted* sense, since the grain orientations were chosen randomly but the morphology was set a priori to be equiaxed [29]. The generation of fully random microstructures would require grains with both random orientation and morphology (see [30] for details). However, for our purposes, the above restricted random procedure allows us to reduce the number of configurations needed to obtain an isotropic ensemble response.

With this in mind, and in order to compare macroscopic and per-phase quantities obtained from FFT simulations with analogous quantities obtained from SC formulations for aggregates with random microstructure, 50 different periodic unit cells have been constructed as follows. First, the grains of the 3-D array described above were numbered from 1 to 512. Next, 50 random sequences of 512 Euler triplets were generated. Each of these sequences was scanned to find the orientations being at minimum distance (in orientation space) from certain 45 special Euler triplets. The latter special orientations essentially cover the orientation space and were pre-selected for ensemble averaging of the per-phase statistical quantities. The orientations at minimum distances from the above special triplets were replaced by the corresponding pre-selected orientations. In this way, those 45 Euler triplets were present in every unit cell, surrounded by different environments, which in turn were randomly chosen. Finally, to construct the αth configuration, the first triplet of the αth random sequence was assigned to grain #1, the second angle to grain #2, and so on.

Using the superscript [α] to denote a single configuration, i.e. $\bar{\boldsymbol{\varepsilon}}^{[\alpha]} = \langle \boldsymbol{\varepsilon}^{[\alpha]} \rangle$ and $\bar{\boldsymbol{\sigma}}^{[\alpha]} = \langle \boldsymbol{\sigma}^{[\alpha]} \rangle$, the ensemble averages of macroscopic magnitudes are given by

$$\bar{\boldsymbol{\varepsilon}} = \frac{1}{N_\alpha} \sum_{\alpha=1}^{N_\alpha} \bar{\boldsymbol{\varepsilon}}^{[\alpha]}, \quad \bar{\boldsymbol{\sigma}} = \frac{1}{N_\alpha} \sum_{\alpha=1}^{N_\alpha} \bar{\boldsymbol{\sigma}}^{[\alpha]}, \qquad (22)$$

where N_α is the number of unit cell configurations. The ensemble averages of per-phase and overall first and second moments are made consistent with prior definitions.

To close this section, let us briefly mention some relevant numerical features of the present approach, namely: (1) the convergence of the FFT method for a

single RVE configuration and (2) the stabilization of the ensemble averaging procedure. In what concerns the first aspect, for a single RVE configuration, the error indicators given by expressions (21) decrease monotonically, for every case considered below. However, reaching errors smaller than a given threshold would require to increase the number of iterations as the contrast of properties (i.e. the anisotropy) at single crystal level and/or the nonlinearity of the material increase. Therefore, as in [13], rather than adopting a unique threshold error, we have chosen to fix an appropriate number of iterations for each set of material properties considered, so that the resulting errors remain low. The number of iterations adopted and the average errors obtained are given in next section, for each material and contrast considered. Finally, concerning the number of configurations adopted here to obtain representative ensemble averages, in [13] we found that, in general, 50 configurations are enough to average out roughly the influence of the different grain environments, resulting in ensemble averages of the per-phase moments that are mainly dictated by the grain orientation.

5. Results and discussion

In this section, the self-consistent approximation discussed in Section 3 will be used to generate estimates for the effective behavior and field fluctuations in untextured (isotropic) polycrystals with FCC and HCP single-crystal grains, undergoing uniaxial tension. Note that throughout this work we will only report results for uniaxial loading cases, leaving the study of the influence of the third stress invariant for future work. These SC estimates will be compared with the results of full-field numerical simulations using the FFT technique, as discussed in Section 4. Results will be presented first for linearly viscous polycrystals with FCC and HCP grains. In spite of the fact that the value of the exponent $n = 1$ is unrealistic for most materials, the comparisons to be made are useful because they serve to assess the accuracy of the standard self-consistent approximation [1,2]. Once this is accomplished, results will be presented for two nonlinear examples, the objective being to compare the predictions of the various nonlinear extensions of the self-consistent approximation, including the 'incremental', 'tangent', 'affine', 'variational', 'second-order NF' and 'second-order' approximations, with the corresponding FFT simulations.

5.1. Linear FCC polycrystals

As is well known, the deformation in FCC single crystals takes place through slip on a set of four slip planes of the type $\{111\}$, along three slip directions

(per plane) of type $\langle 110 \rangle$. The existence of these 12 slip systems ensures that there are five linearly independent systems, allowing arbitrary (incompressible) plastic deformation for the grains. The crystals are assumed to have linearly viscous behavior characterized by relations (4) with $n = 1$, and with identical slip flow stresses so that $(\tau_0)_{(k)} = \tau_0$ for all $k = 1, \ldots, 12$. The polycrystal is assumed to be untextured, with isotropic two-point statistics, corresponding to 'equiaxed' grains. The behavior of such a polycrystal is linear and can then be characterized in terms of the effective flow stress $\tilde{\sigma}_0$ introduced in expression (5). In addition, results are presented for the overall standard deviations of the equivalent stress and strain-rate, as well as the corresponding per-phase averages, and per-phase standard deviations defined by Eq. (7).

The overall properties obtained for both the SC approximation and the FFT simulations are summarized in Table 1. Note that the FFT results correspond to averages over 50 configurations and that each individual simulation consisted in 30 iterations, resulting in ensemble average relative errors (defined as the mean values of the relative errors given by expressions (21) over the 50 configurations) of 0.119×10^{-4} and 0.162×10^{-4}, for the stress and strain-rate fields, respectively. It is worth mentioning that the dispersion of the above relative errors was low, with range/mean values (i.e. $[\max(\cdot) - \min(\cdot)]/\langle \cdot \rangle$) of 14.3% and 8.6%, respectively. For this low-anisotropy system, it can be seen that the agreement between the FFT and SC estimates is excellent for the effective flow stress, and quite good for the overall standard deviations of the stress and strain-rates. In this respect, it is worth noting that the standard deviations obtained with FFT would be expected to be more susceptible to numerical error, being higher-order statistical quantities.

The orientation-dependence of the phase-averages and fluctuations of the stress and strain-rate fields over grains with given, fixed orientations is considered next. Given the symmetries already alluded to, it is sufficient to restrict attention to the standard spherical triangle, with vertices $\{100\}$, $\{100\}$ and $\{111\}$. (Note that equal-area projections are used). Then, the various points in the spherical triangle correspond to grains which are so oriented relative to the loading axis. Thus, for example, the point $\{100\}$ corresponds to grains that are oriented such that the loading axis is aligned with the $\{100\}$ direction in these grains.

Table 1
Self-consistent and FFT estimates for the effective flow stress and overall field fluctuations of linear, isotropic FCC polycrystals

	$\tilde{\sigma}_0/\tau_0$	$SD(\sigma_e)/\bar{\sigma}_e$	$SD(\epsilon_e)/\bar{\epsilon}_e$
SC	1.5	0.408	0.333
FFT	1.499	0.423	0.324

In Fig. 1, plots are given for the per-phase averages of the von Mises stress, $\bar{\sigma}_e^{(r)}$, and the equivalent plastic strain-rate, $\bar{\varepsilon}_e^{(r)}$. The SC estimates are shown on the left and the FFT on the right. It can be observed from these figures that the average stress is largest for orientations in the vicinity of the {111} direction, and lowest near the {100} direction, with roughly the opposite behavior for the strain-rate. Although the FFT and SC estimates are in very good qualitative agreement, there are some minor differences in the results, such as some extra features in the FFT level curves, which are not present in the SC, and which are probably due to numerical inaccuracies. There are also some differences in the maximum and minimum values (refer to Table 2 for details).

Concerning the per-phase standard deviations of the equivalent stress and strain fields, it is recalled [31] that the SC method yields a uniform value for these quantities. On the other hand, the corresponding FFT predictions exhibit some scatter about the SC prediction. The maximum, average and minimum FFT and unique SC values are also given in Table 2. It can be seen that the average values match fairly well, and that the scatter of the values in the FFT simulations is relatively small (less than 5%), which shows that the uniformity of the fluctuations may be a good approximation in this case. Certainly part of the scatter is due to numerical error in computing these higher-order quantities, but it is also probable that the per-phase standard deviations in
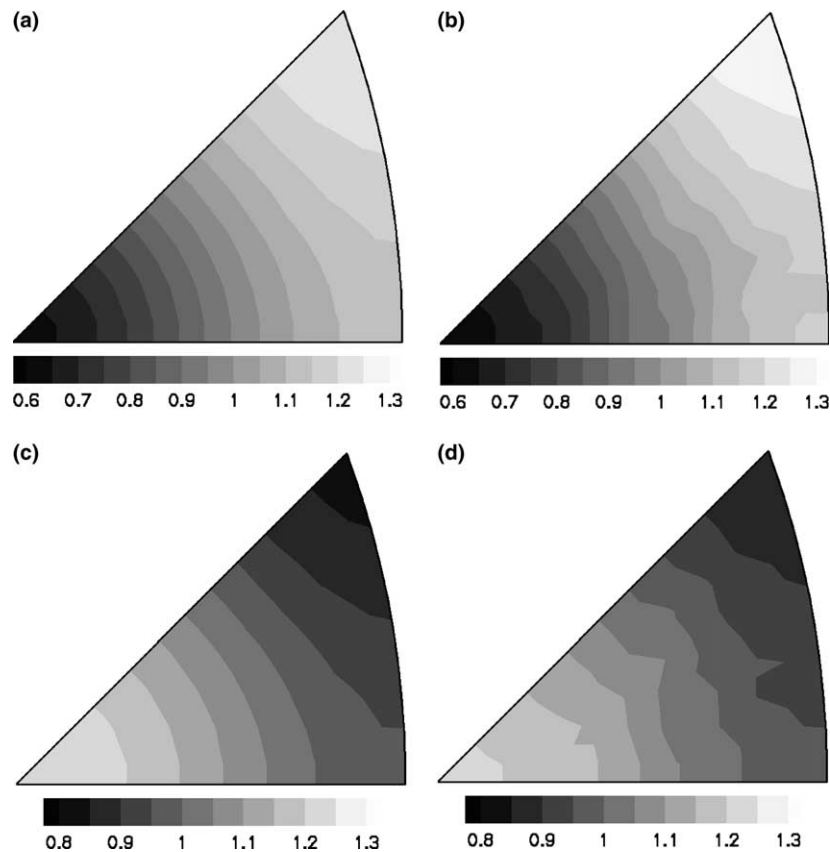

Fig. 1. Plots of the SC (left) and FFT (right) estimates for the per-phase averages of the von Mises stress and the plastic equivalent strain-rate, as function of orientation in the spherical triangle, for linear, isotropic FCC polycrystals. Parts (a) and (b) are for the stress averages $\bar{\sigma}_e^{(r)}$, normalized by the applied stress $\bar{\sigma}_e$, and (c) and (d) for the strain-rates $\bar{\varepsilon}_e^{(r)}$, normalized by $\bar{\varepsilon}_e$.

Table 2
Self-consistent and FFT results for the per-phase average and fluctuations of the stress and strain-rate fields for linear, isotropic FCC polycrystals

	SC			FFT		
	Minimum	Average	Maximum	Minimum	Average	Maximum
$\bar{\sigma}_e^{(r)}/\bar{\sigma}_e$	0.642	1.034	1.245	0.627	1.038	1.282
$\bar{\varepsilon}_e^{(r)}/\bar{\varepsilon}_e$	0.839	1.015	1.244	0.857	1.014	1.207
$SD(\sigma_e^{(r)})/\bar{\sigma}_e$	0.270	0.270	0.270	0.253	0.266	0.278
$SD(\varepsilon_e^{(r)})/\bar{\varepsilon}_e$	0.264	0.264	0.264	0.249	0.261	0.272

actual polycrystals would not be exactly uniform in general.

5.2. Linear HCP polycrystals

In this section, we consider hexagonal-close-packed (HCP) polycrystalline materials with c/a ratios of 1.593 and 1.629, which are thought to be reasonable values for Zr and ice. The value of n is again chosen to be equal to 1, corresponding to linearly viscous behavior. Although this value is unrealistic for Zr and ice, it will be used here to explore the validity of the self-consistent approximation for these materials, as determined by comparisons with FFT simulations for the same materials. In particular, the effect of grain heterogeneity, which can be significant for these materials, will be investigated. In the next section, a more realistic value ($n = 3$) will be considered for ice polycrystals. The relevant slip systems are basal slip ($\{0001\}\langle11\bar{2}0\rangle$), prismatic slip ($\{10\bar{1}0\}\langle11\bar{2}0\rangle$), and first-order ($\{10\bar{1}1\}\langle11\bar{2}3\rangle$) and second-order ($\{11\bar{2}2\}\langle11\bar{2}3\rangle$) pyramidal-$\langle c + a\rangle$ slip, which will be denoted by the labels A, B, and C, respectively. Note that the three basal plus the three prismatic systems supply only four (two each) linearly independent systems, allowing no straining along the $\langle c\rangle$-axis. However, the 12 first-order pyramidal-$\langle c + a\rangle$ systems, and the six second-order pyramidal-$\langle c + a\rangle$ systems each contain sets of five independent systems.

The polycrystals are again assumed to be untextured, with isotropic two-point statistics. Using the flow shear stress on the basal systems τ_A as a reference, we consider two cases: (a) for the Zr-type material, the reference stress of the prismatic systems is taken to be equal to that of the basal systems ($\tau_B = \tau_A$), and that of the 'first-order' pyramidal systems is considered to be variable ($\tau_C = M\tau_A$, where the 'contrast parameter' or 'grain anisotropy factor' M is variable); (b) for the ice-type material, the reference stress of the prismatic systems is taken to be equal to that of the 'second-order' pyramidal systems ($\tau_B = \tau_C$), and variable ($\tau_C = M\tau_A$, with M variable). Note that for the first class of materials, there are four independent slip systems left in the limit as M tends to infinity (no pyramidal slip), while for the second class, only two systems are left in the limit as M tends to

infinity (no prismatic and no pyramidal). Therefore, the second class of materials is kinematically more constrained than the first, even if both—unlike the FCC materials considered earlier—violate the von Mises rule (which states that five independent systems are required to accommodate a general plastic deformation in single crystals) in the limit as $M \to \infty$. For the above two types of linear HCP polycrystals, Table 3 shows the number of iterations adopted in each individual FFT simulation, as well as the resulting ensemble average stress and strain-rate relative errors, for a sample of different values of the contrast parameter M. It is worth mentioning that the dispersion of the relative errors over the 50 configurations remain low, even for large contrasts, e.g. for $M = 1000$ we obtained, in the Zr-like case, range/mean dispersions of 18.1% and 9.7% for the stress and strain-rate relative errors, respectively, and of 18.9% and 22.1% for the ice-like polycrystal case.

In Fig. 2(a), the SC estimates and the FFT results for the effective flow stress $\tilde{\sigma}_0$ of the Zr-type polycrystal are plotted as functions of the grain anisotropy M. It can be seen that the SC and numerical results are in very good quantitative agreement, even for very large values of M. However, perhaps more importantly, the FFT simulations seem to corroborate the SC prediction that the polycrystal will exhibit a finite flow stress in the limit as M tends to infinity. This is significant because it shows that the von Mises rule need not hold for an isotropic polycrystal: even though the single crystals cannot accommodate arbitrary deformations, isotropic polycrystals of these HCP materials will be able to accommodate general deformations (as first suggested by Hutchinson [32]). In Fig. 2(b), plots are shown for the SC and FFT estimates for the standard deviations of the von Mises stress and equivalent plastic strain-rate, SD(σ_e) and SD(ε_e), as functions of the grain anisotropy M. These results are normalized by the average von Mises stress $\bar{\sigma}_e$ and equivalent plastic strain-rate $\bar{\varepsilon}_e$, respectively. It can be seen that the agreement between the SC and FFT predictions is very good for the strain-rate fluctuations, and quite good for the stress fluctuations, except for very large values of M, when they begin to deviate. The observed differences for large values of M could be due in part to numerical errors in the FFT simulations, which would require very fine

Table 3
Number of iterations adopted in each individual FFT simulation, and ensemble averages of the stress and strain-rate field relative errors, for untextured linearly viscous Zr-type and ice-type polycrystals, for different values of the contrast parameter M

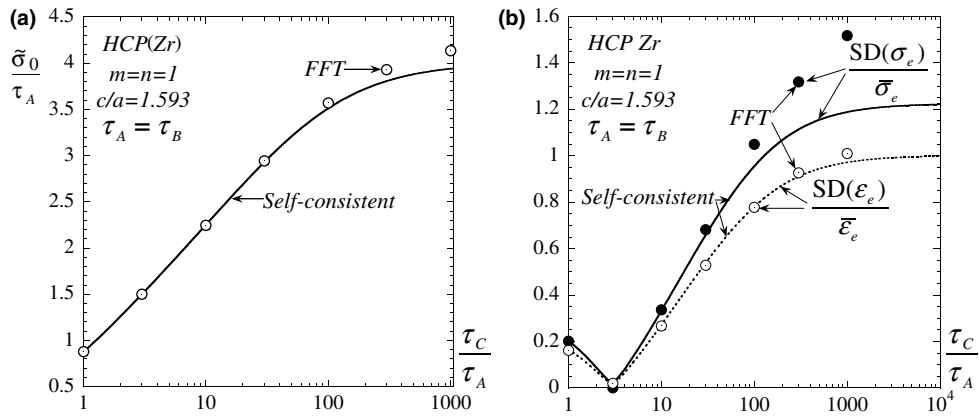| M	Zr-type			Ice-type		
	Iterations	$\langle\mathrm{err}(\boldsymbol{\sigma})\rangle$	$\langle\mathrm{err}(\boldsymbol{\varepsilon})\rangle$	Iterations	$\langle\mathrm{err}(\boldsymbol{\sigma})\rangle$	$\langle\mathrm{err}(\boldsymbol{\varepsilon})\rangle$
1	20	0.493×10^{-4}	0.724×10^{-4}	20	0.308×10^{-4}	0.457×10^{-4}
10	30	0.715×10^{-4}	0.975×10^{-4}	40	0.619×10^{-5}	0.722×10^{-5}
100	60	0.215×10^{-3}	0.984×10^{-4}	80	0.480×10^{-4}	0.40×10^{-4}
1000	100	0.666×10^{-3}	0.402×10^{-4}	120	0.127×10^{-3}	0.995×10^{-4}

Fig. 2. Plots of the effective flow stress and field fluctuations for untextured, linearly viscous ($n = 1$) Zr-type polycrystals with 'equiaxed' grains and $\tau_B = \tau_A$, as functions of the grain anisotropy τ_C/τ_A: (a) the effective flow stress $\tilde{\sigma}_0$, normalized by the slip stress τ_A; (b) overall standard deviations of the von Mises stress SD(σ_e), and the equivalent plastic strain-rate SD(ε_e), normalized by the applied stress $\bar{\sigma}_e$, and the applied strain-rate $\bar{\varepsilon}_e$, respectively.

meshes to resolve accurately the very large fluctuations that would be expected in the fields as a consequence of the strong heterogeneity in the polycrystal for the larger values of M. However, it is also possible that the linear SC scheme simply is not able to reproduce correctly higher-order moments of the fields for large grain anisotropy. In spite of the quantitative differences between the SC and FFT estimates, the results seem to suggest that the (suitably normalized) fluctuations tend to saturate for large enough values of M. It is also noted, in passing, that the fluctuations go to zero for a value of M approximately equal to 3, which happens to correspond to isotropic behavior for the constituent single crystals.

In Fig. 3(a), the corresponding SC and FFT estimates for the effective flow stress $\tilde{\sigma}_0$ of untextured, ice-type polycrystals are plotted as functions of the grain anisotropy M. Note again that the two types of results are in

excellent quantitative agreement, even for very large values of M. In this case, however, the effective flow stress is seen to grow linearly with M, which is very different from the previous case, where the effective flow stress was seen to tend to saturate for large enough values of M. Therefore, this example shows that two independent slip systems for the constituent single-crystals are not sufficient to ensure that the isotropic polycrystal will be able to accommodate arbitrary deformations. In Fig. 3(b), plots are shown for the SC and FFT estimates for the overall standard deviations of the stress and strain-rate, SD(σ_e) and SD(ε_e), as functions of the grain anisotropy M. These results are normalized by $\bar{\sigma}_e$ and $\bar{\varepsilon}_e$, respectively. It can again be seen that the agreement between the SC and FFT predictions is very good, even though this time it is better for the stress than for the strain-rate fluctuations, which start to deviate for very large values of M. Nevertheless, quantitative
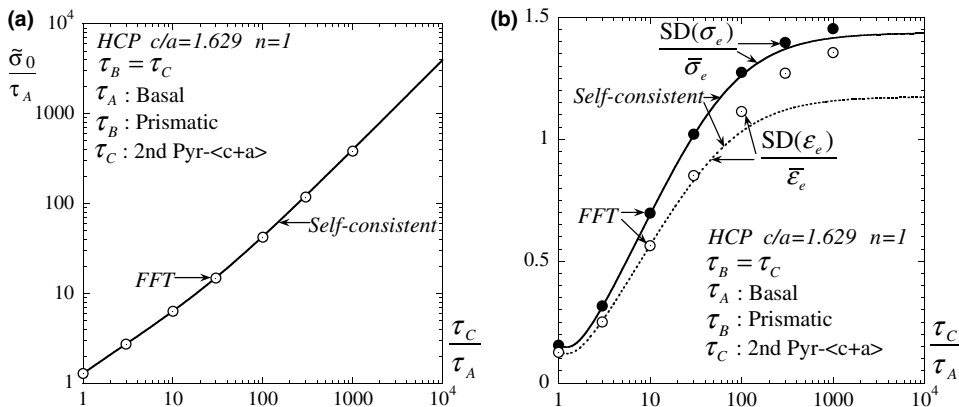

Fig. 3. Plots of the effective flow stress and field fluctuations for untextured, linearly viscous ($n = 1$) ice-type polycrystals with 'equiaxed' grains and $\tau_B = \tau_C$, as functions of the grain anisotropy τ_C/τ_A: (a) the effective flow stress $\tilde{\sigma}_0$, normalized by the slip stress τ_A; (b) overall standard deviations of the von Mises stress SD(σ_e), and the equivalent plastic strain-rate SD(ε_e), normalized by the applied stress $\bar{\sigma}_e$, and the applied strain-rate $\bar{\varepsilon}_e$, respectively.

differences aside, the results seem to suggest that, as was the case for polycrystals with four independent slip systems, the (suitably normalized) fluctuations for the present case involving two independent slip systems case also tend to saturate for large enough values of M.

The orientation-dependence of the phase-averages and fluctuations of the stress and strain-rate fields for grains with given, fixed orientations is investigated next. Given the symmetries already alluded to, it is sufficient to restrict attention to a spherical triangle, this time with vertices $\{0001\}$, $\{1\bar{2}\bar{1}0\}$ and $\{1\bar{1}00\}$. Then, a given orientation in this triangle corresponds to grains that are oriented such that the loading axis is aligned with such a direction in the grains. Figs. 4 and 5 show the per-phase averages of the von Mises stress $\bar{\sigma}_e^{(r)}$, and the equivalent plastic strain-rate $\bar{\dot{\varepsilon}}_e^{(r)}$, respectively, for various values of the grain anisotropy parameter $M = \tau_C/\tau_A$ (1, 10, 100), for the case of Zr-type linear polycrystals. It can be seen from these figures that the average strain-rate is largest for a band intermediate between the $\{0001\}$ and $\{1\bar{1}00\}$ directions, except for the case $M = 1$ when the largest values is for the $\{0001\}$ direction. Note that the average strain-rate along this direction actually becomes a pronounced minimum as the value of M is increased, which is not surprising in view of the fact that the grains become rigid along the c-axis, as M is increased. It is also noted that the corresponding behavior for the stress averages is roughly the opposite of that of the strain-rates for all values of M. On the other hand, while the overall agreement between the

SC and FFT predictions is quite good, there are some quantitative differences in these predictions, especially for the higher value of M. For more details on the differences between these two types of estimates, refer to Table 4. However, the somewhat irregular patterns in the FFT results suggest again that these estimates may become inaccurate for the fluctuations at the larger values of M.

As already discussed in the context of the FCC polycrystals, the SC method also yields a uniform value for the per-phase standard deviations of the equivalent stress and strain fields in the HCP polycrystals. The corresponding FFT predictions exhibit some scatter about the SC prediction. The maximum, average and minimum values of the FFT estimates are compared with the SC values in Table 4 for a value of $M = 10$. It can be seen that the average values match reasonably well (less than 10% differences), except for the stress fluctuations for $M = 100$ (not shown), when the differences are much larger.

5.3. Nonlinear FCC polycrystals

In this section, the same class of isotropic FCC polycrystals of Section 5.1 is considered, but now with a more realistic nonlinear exponent ($n = 10$). Estimates of the SC type were computed for the effective flow stress $\tilde{\sigma}_0$, as well as for the overall standard deviations of the equivalent stress and strain-rate fields, using the 'incremental' [5,6] 'tangent' [7,8], 'affine' [21], 'variational'
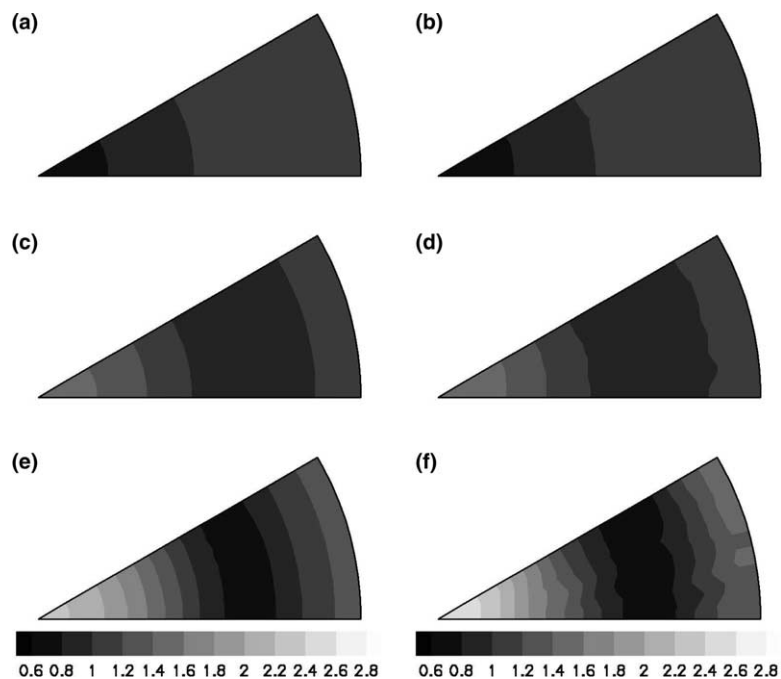

Fig. 4. Plots of the SC and FFT estimates for the per-phase averages of the von Mises stress $\bar{\sigma}_e^{(r)}$ are shown on the left- and right-hand sides, respectively, as function of orientation in the spherical triangle, for isotropic Zr-type polycrystals with $\tau_A = \tau_B$ and $\tau_C/\tau_A = M$. The results are normalized by the applied stress $\bar{\sigma}_e$. Parts (a) and (b), (c) and (d), and (e) and (f) correspond to the following values of M: 1, 10, 100.
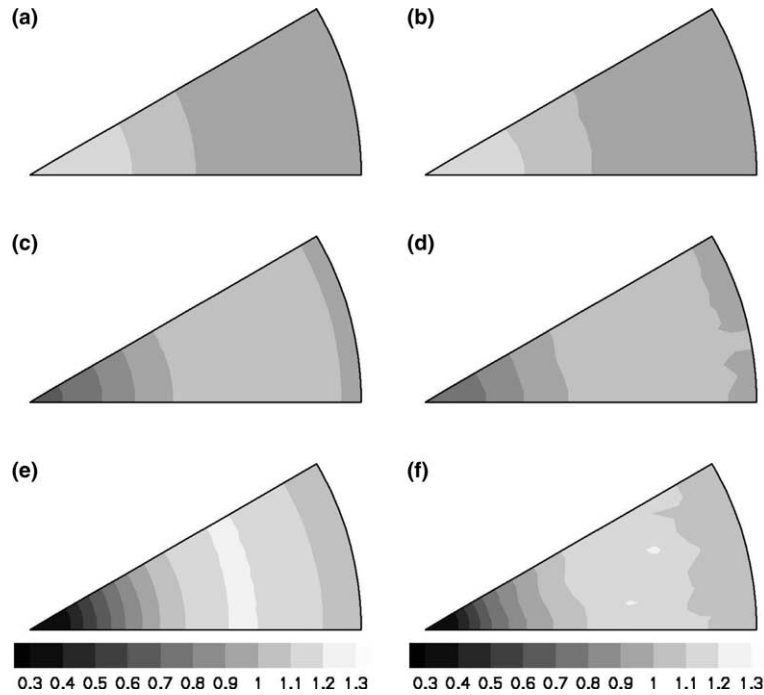
Fig. 5. Plots of the SC and FFT estimates for the per-phase averages of the equivalent plastic strain-rate $\bar{\varepsilon}_{\rm e}^{(r)}$ are shown on the left- and right-hand sides, respectively, as function of orientation in the spherical triangle, for isotropic Zr-type polycrystals with $\tau_{\rm A} = \tau_{\rm B}$ and $\tau_{\rm C}/\tau_{\rm A} = M$. The results are normalized by the applied strain-rate $\bar{\varepsilon}_{\rm e}$. Parts (a) and (b), (c) and (d), and (e) and (f) correspond to the following values of M: 1, 10, 100.

Table 4
Self-consistent and FFT results for the per-phase average and fluctuations of the stress and strain-rate fields for linear, isotropic Zr-type polycrystals with $M = 10$

	SC			FFT		
	Minimum	Average	Maximum	Minimum	Average	Maximum
$\bar{\sigma}_{\rm e}^{(r)}/\bar{\sigma}_{\rm e}$	0.872	1.021	1.474	0.855	1.027	1.547
$\bar{\varepsilon}_{\rm e}^{(r)}/\bar{\varepsilon}_{\rm e}$	0.696	1.011	1.086	0.728	1.007	1.079
$\mathrm{SD}(\sigma_{\rm e}^{(r)})/\bar{\sigma}_{\rm e}$	0.216	0.217	0.218	0.199	0.216	0.245
$\mathrm{SD}(\varepsilon_{\rm e}^{(r)})/\bar{\varepsilon}_{\rm e}$	0.213	0.213	0.213	0.196	0.209	0.232

[15,16], 'second-order NF' (without fluctuations) [20] and 'second-order' (with fluctuations) [17,18] methods. In addition, the Taylor upper and Reuss lower bounds are also provided for reference purposes. These bounds and SC estimates are compared in Table 5 with the corresponding results from the FFT simulations. The FFT results shown correspond to averages over 50 configurations, where each individual simulation consisted in 100 iterations. This resulted in ensemble-average relative errors for the stress and strain-rate fields of 0.123×10^{-3} and 0.504×10^{-4} and range/mean dispersions of 47.3% and 41.1%, respectively.

The main observation from Table 5 is that the both 'second-order' models appear to give the best overall agreement with the corresponding FFT results. Thus, the 'second-order' estimate for $\tilde{\sigma}_0$ is lower than the FFT result (2.540 vs. 2.614), while the estimates for the overall fluctuations of the stress and strain-rate are lower and higher, respectively (0.413 vs. 0.480,

Table 5
Taylor, Reuss, different self-consistent, and FFT estimates of the effective flow stress and the overall field SDs for a nonlinear, isotropic FCC polycrystal ($n = 10$)

Model	$\tilde{\sigma}_0/\tau_0$	$\mathrm{SD}(\sigma_{\rm e})/\bar{\sigma}_{\rm e}$	$\mathrm{SD}(\epsilon_{\rm e})/\bar{\epsilon}_{\rm e}$
Taylor	2.905	0.568	0
Reuss	2.201	0	0.825
Incremental	2.880	0.752	0.185
Affine	2.741	0.576	0.752
Tangent	2.617	0.349	0.947
Variational	2.811	0.696	0.188
Second-order NF	2.582	0.576	0.752
Second-order	2.540	0.413	0.878
FFT	2.614	0.480	0.586

and 0.878 vs. 0.586). On the other hand, the 'second-order NF' estimate actually appears to give a slightly better prediction for $\tilde{\sigma}_0$, as well as for the strain-rate

fluctuations, but somewhat worse for the stress fluctuations. Also note that while the affine SC estimate gives the same predictions for the stress and strain-rate fluctuations as the 'second-order NF' estimate, the agreement with the FFT for the effective flow stress is worse. It is further noted that the 'tangent' SC estimate for the effective flow stress is in excellent agreement with the FFT result, but the corresponding estimates for the fluctuations are not as good. Finally, it is noted, for completeness, that the 'second-order NF' model gives a prediction for the effective flow stress that is close to the corresponding tangent estimate at this value of n. However, very significant differences were observed [33] for larger values of n, with the tangent estimate tending to the Reuss lower bound as $n \to \infty$.

5.4. Ice polycrystals

This section is concerned with ice polycrystals at -10 °C. At this temperature, the active slip systems are the same as those identified in the previous section for the 'ice-type' polycrystals, but with a more realistic value [34] of the creep exponent ($n = 3$). This problem was considered by Hutchinson [32] using the 'incremental' version of the self-consistent approximation, and by Castelnau et al. [35,36] using the corresponding 'tangent' version.

In Fig. 6, several nonlinear extensions of the self-consistent approximation for the effective flow stress $\tilde{\sigma}_0$ of untextured, power-law ($n = 3$) ice polycrystals with $\tau_B = \tau_C$ are plotted as functions of the grain anisotropy $M = \tau_C/\tau_A$. The predictions of the various nonlinear SC methods are compared with the corresponding FFT estimates, as well as the Taylor upper bound and Reuss lower bound. Details on the convergence of the FFT calculations (number of iterations, average errors) are given in Table 6 for different values of the contrast M. Fig. 6(a) gives the results in linear scales, while in

Table 6
Number of iterations adopted in each individual FFT simulation, and ensemble averages of the stress and strain-rate field relative errors, for ice polycrystals ($n = 3$), for different values of the contrast parameter M

M	Iterations	$\langle \text{err}(\sigma) \rangle$	$\langle \text{err}(\varepsilon) \rangle$
1	30	0.277×10^{-4}	0.131×10^{-4}
10	100	0.492×10^{-4}	0.266×10^{-4}
50	250	0.255×10^{-4}	0.118×10^{-4}
80	400	0.102×10^{-3}	0.392×10^{-4}

Fig. 6(b) same results are plotted in logarithmic scales. It can be seen from these figures that in fact the two 'second-order' SC estimates give the best overall agreement with the FFT predictions, with the more recent version incorporating fluctuations yielding the most accurate results. The 'variational' estimate gives somewhat larger predictions, which is consistent with its upper bound status [37]. On the other hand, the 'affine' estimates almost coincide with the 'variational' results (note that this is not a general result), while the 'incremental' and Taylor models are much stiffer, leading to significant errors relative to the FFT estimates for the larger values of M. Finally, the 'tangent' model, while very accurate for the lower value of M (up to about 10), severely underestimates the overall behavior for the larger values of M, giving less than half of the FFT value for $M = 80$. Note that this estimate exhibits a behavior similar to the Reuss bound, in that it predicts a saturation of the effective behavior for large enough values of M, in contrast with the other estimates which give linear growth with M.

In Fig. 7(a), plots are shown for the overall standard deviations of the stress field, $\text{SD}(\sigma_e)$, normalized by $\bar{\sigma}_e$, as functions of the grain anisotropy $M = \tau_C/\tau_A$. Here, once again, the different SC estimates are compared with the FFT results, as well as with the Taylor and Reuss estimates. It can be seen that the 'variational' and 'second-order' estimates, as well as the 'second-order NF' and 'affine' models (which coincide) give the best overall
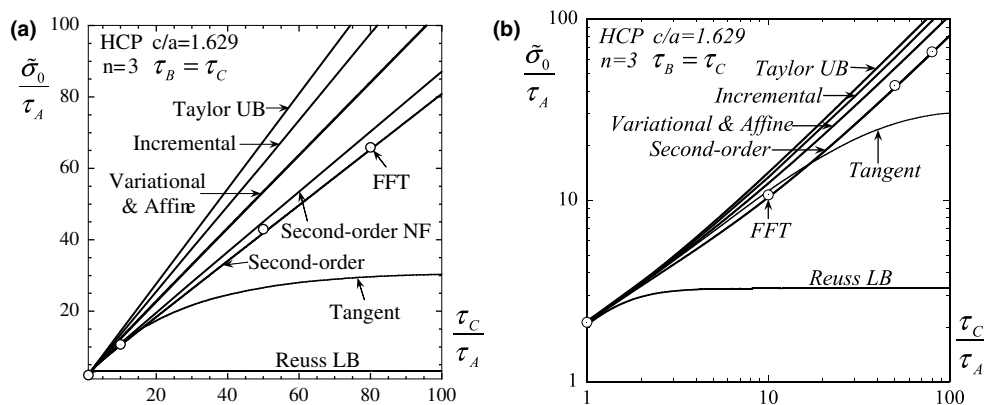

Fig. 6. Plots of various self-consistent estimates and FFT simulations for the effective flow stress $\tilde{\sigma}_0$, normalized by the slip stress τ_A, for untextured, power-law ($n = 3$) ice polycrystals with 'equiaxed' grains and $\tau_B = \tau_C$, as functions of the grain anisotropy τ_C/τ_A: (a) linear scales; (b) log scales.
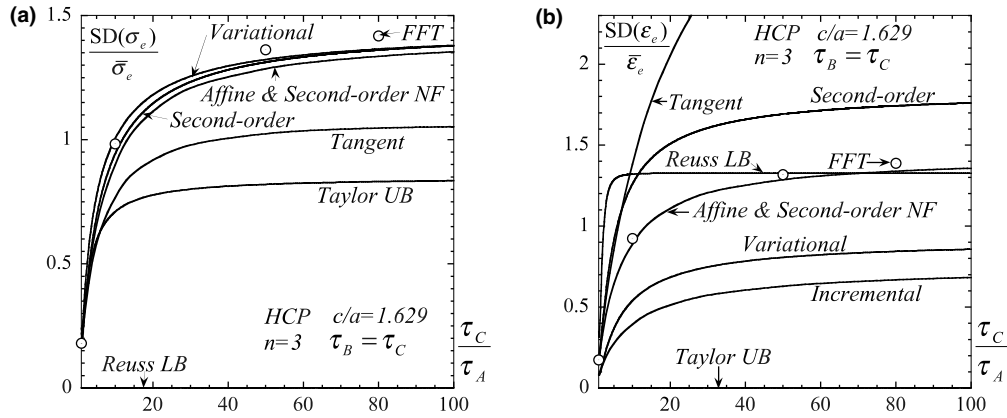
Fig. 7. Plots of various self-consistent estimates and FFT simulations for the field fluctuations for untextured, power-law ($n = 3$) ice polycrystals with 'equiaxed' grains and $\tau_B = \tau_C$, as functions of the grain anisotropy τ_C/τ_A: (a) overall standard deviations of the von Mises stress $SD(\sigma_e)$, normalized by $\bar{\sigma}_e$; (b) overall standard deviations of the equivalent plastic strain-rate $SD(\varepsilon_e)$, normalized by $\bar{\varepsilon}_e$.

agreement with the FFT predictions. Not only is the qualitative behavior similar, predicting saturation of the fluctuations for large values of M, but they also do a good job in terms of quantitative agreement. The 'tangent', Taylor and Reuss estimates, on the other hand, underestimate the behavior of the stress fluctuations, with the Reuss estimate of course giving zero fluctuations. It is also worth noting that 'incremental' model (not shown for the sake of clarity) almost coincide with the 'affine' and 'second-order NF' predictions in this case.

Fig. 7(b) gives the corresponding results for the strain-rate fluctuations, $SD(\varepsilon_e)$, normalized by $\bar{\varepsilon}_e$. While the 'tangent' and the 'incremental' formulations severely overestimate and underestimate, respectively, the full-field predictions, the 'affine' and 'second-order NF' models show the best agreement with the FFT results. On the other hand, the 'second-order' predictions capture the large-M qualitative trend, but they are systematically larger than the FFT results. This better performance of the 'affine/second-order NF' over the 'second-order' seems to contradict the former result on the effective flow stress, for which the opposite was found. We suspect that this apparent contradiction may be due to the fact that the resolution of the FFT grid may not be fine enough to be able to generate accurate results for the strain field fluctuations, since the strain fields are expected to be highly oscillating within each grain.

Concerning the rest of the fluctuation results, the 'variational' model also underestimates the magnitude of the fluctuations. The Reuss estimate is seen to do rather well in predicting the rough magnitudes involved, but gives a rather sharp transition to a saturating value, which is not observed in the FFT simulation results. Moreover, it is recalled here that the Reuss predictions consist only of (most probably overestimated) intergranular strain-rate fluctuations associated with the uniform stress assumption, while in reality the field fluctuations are a combination of intergranular and intragranular effects. Finally, the Taylor estimate for the strain-rate fluctuations vanishes identically, in agreement with the uniform strain-rate hypothesis involved in these estimates.

For these nonlinear polycrystals, the SC estimates no longer give uniform predictions for the per-phase standard deviations of the equivalent stress and strain. When compared with the FFT predictions, the general patterns are roughly similar, apart from some 'noisy' features in the FFT, which can be attributed to numerical errors. However, as already pointed out in the context of Fig. 7 there are significant differences in the magnitudes of the average strain-rates predicted by the 'second-order' SC estimates and FFT simulations. A general comparison between the maximum, average and minimum values of the FFT estimates is summarized in Table 7 for a value of $M = 10$.

Table 7
Second-order self-consistent estimates and FFT results for the per-phase average and fluctuations of the stress and strain-rate fields for isotropic ice polycrystals with $n = 3$ and $M = 10$

	SC			FFT		
	Minimum	Average	Maximum	Minimum	Average	Maximum
$\bar{\sigma}_e^{(r)}/\bar{\sigma}_e$	0.883	1.153	1.423	0.886	1.197	1.515
$\bar{\varepsilon}_e^{(r)}/\bar{\varepsilon}_e$	0.553	1.138	1.598	0.659	1.065	1.364
$SD(\sigma_e^{(r)})/\bar{\sigma}_e$	0.635	0.723	0.803	0.605	0.734	0.823
$SD(\varepsilon_e^{(r)})/\bar{\varepsilon}_e$	1.046	1.074	1.093	0.769	0.817	0.853

6. Concluding remarks

In this work, the self-consistent method has been used to generate estimates for the effective behavior, as well as for the fluctuations of the stress and strain-rate fields in linear and power-law viscous polycrystals with isotropic microstructures. These theoretical estimates were compared with the results of FFT simulations performed on ensembles of random polycrystals, with the objective of assessing the accuracy of self-consistent approximation for these materials.

For linear polycrystals, it was found that the standard self-consistent method [1,2] gives accurate estimates for the effective behavior, when compared with the FFT simulations. As for the field fluctuations, the matching between the SC estimates and the FFT simulations is very good for moderate grain anisotropies, but starts to deteriorate at higher contrasts.

For power-law viscous polycrystals, the use of the SC approximation for the relevant 'linear comparison polycrystal' in the context of the 'second-order' homogenization method [17,18] leads to the best overall agreement with the FFT results for the effective behavior—at least when compared with the 'incremental', 'affine', 'tangent' and 'variational' extensions of the SC approximation, especially for high grain anisotropies. Concerning the overall field fluctuations, the 'second-order' results exhibit good qualitatively agreement with the full-field predictions, but the results of an earlier version of the method (NF: without fluctuations) match better with the above FFT results—especially those corresponding to the strain-rate field fluctuations at large contrasts. This unexpected result could be attributed, at least in part, to numerical inaccuracies of the FFT results, in turn due to the development at large grain anisotropies of highly localized deformation fields that would require more refined meshes, than those allowed by our computational resources. Further work will be required to elucidate this point.

Concerning the effect of grain anisotropy, it was found that the effective behavior of the polycrystals was sensitive to the number of independent slip systems that are active at the single-crystal level. Thus, for ice-type polycrystals, which exhibit easy slip only on the basal systems (forming a set of two independent systems), the effective flow stress was found to grow proportionally to the flow stress of the hard prismatic and pyramidal systems. On the other hand, for Zr-type polycrystals, which exhibit easy slip on the basal and prismatic systems (forming a set of four independent systems), the effective flow stress was found to saturate, after some growth, with increasing values of the hard pyramidal systems. Although, of course, the effective behavior was found to be dependent on the strain-rate sensitivity, the just-mentioned scaling behavior for large grain anisotropy [37] was found to be independent of the strain-rate sensitivity. Grain anisotropy was also found to have an effect on both the overall stress and strain-rate fluctuations, tending to increase with increasing grain anisotropy, but then saturating for large enough anisotropy. This is consistent with the physics of the problem requiring that certain components of the stress and strain tensors be continuous across grains with different orientations, which lead to the presence of highly nonuniform fields within the grains. In addition to the overall fluctuations, estimates were also generated for the per-phase averages and fluctuations of the stress and strain-rate fields in the polycrystal. It was found that the per-phase averages depend on the orientation of the grain relative to the loading, with the range of observed values increasing with increasing grain anisotropy. However, an interesting behavior was observed for the per-phase standard deviations of the von Mises stress and equivalent strain fields of linear, isotropic polycrystals: the self-consistent model suggests that these quantities are independent of grain orientation [31], and the FFT simulations appear to confirm that this is not a bad approximation for random linear polycrystals with isotropic textures. This result, however, does *not* hold for nonlinear polycrystals. Finally, it is noted that the findings of this paper are completely consistent with the corresponding findings of Lebensohn et al. [13] for a model two-dimensional polycrystal, for which exact results are available in the linear case, as well as rigorous bounds in the nonlinear case.

References

[1] Hershey AV. ASME J Appl Mech 1954;21:236.
[2] Kröner E. Z Physik 1958;151:504.
[3] Willis JR. J Mech Phys Solids 1977;25:185.
[4] Kröner E. J Phys F 1978;8:2261.
[5] Hill R. J Mech Phys Solids 1965;13:89.
[6] Hutchinson JW. Proc R Soc Lond A 1976;348:101.
[7] Molinari A, Canova GR, Ahzi S. Acta Metall Mater 1987;35:2983.
[8] Lebensohn RA, Tomé CN. Acta Metall Mater 1993;41:2611.
[9] Moulinec H, Suquet P. C R Acad Sci Paris II 1994;318:1417.
[10] Moulinec H, Suquet P. Comput Method Appl Mech Eng Sci 1998;157:69.
[11] Michel J, Moulinec H, Suquet P. Comput Modelling Eng Sci 2000;1:79.
[12] Lebensohn RA. Acta Mater 2001;49:2723.
[13] Lebensohn RA, Liu Y, Ponte Castañeda P. Proc R Soc Lond A 2004;460:1381.
[14] Bhattacharya K, Suquet P. 2004, in preparation.
[15] Ponte Castañeda P. J Mech Phys Solids 1991;39:45.
[16] deBotton G, Ponte Castañeda P. Proc R Soc Lond A 1995;448:121.

[17] Ponte Castañeda P. J Mech Phys Solids 2002;50:737.
[18] Liu Y, Ponte Castañeda P. J Mech Phys Solids 2004;52:467.
[19] Ponte Castañeda P, Suquet P. Adv Appl Mech 1998;34:171.
[20] Ponte Castañeda P. J Mech Phys Solids 1996;44:827.
[21] Masson R, Bornert M, Suquet P, Zaoui A. J Mech Phys Solids 2000;48:1203.
[22] Laws N. J Mech Phys Solids 1973;21:9.
[23] Willis JR. Adv Appl Mech 1981;21:1.
[24] Bobeth M, Diener G. J Mech Phys Solids 1987;35:37.
[25] Kreher W. J Mech Phys Solids 1990;38:115.
[26] Parton VZ, Buryachenko VA. Sov Phys Dokl 1990;35(2):191.
[27] Michel J, Moulinec H, Suquet P. Comput Method Appl Mech Eng Sci 1999;172:109.
[28] Michel J, Moulinec H, Suquet P. Int J Numer Method Eng 2001;52:139.

[29] Lebensohn RA, Castelnau O, Brenner R, Gilormini P. Int J Solids Struct, submitted.
[30] Kanit T, Forest S, Galliet I, Mounoury V, Jeulin D. Int J Solids Struct 2003;40:47.
[31] Liu Y, Ponte Castañeda P. J Mech Phys Solids 2004;52:1175.
[32] Hutchinson JW. Met Trans A 1977;8:1465.
[33] Bornert M, Ponte Castañeda P, Zaoui A. J Mech Phys Solids 2001;49:2737.
[34] Duval P, Ashby MF, Anderman I. J Phys Chem 1983;87:4066.
[35] Castelnau O, Duval P, Lebensohn RA, Canova GR. J Geophys Res B 1996;101:13851.
[36] Castelnau O, Canova GR, Lebensohn RA, Duval P. Acta Mater 1997;45:4823.
[37] Nebozhyn MV, Gilormini P, Ponte Castañeda P. J Mech Phys Solids 2001;49:313.